International Journal of Fracture, DOI 10.1007/s10704-011-9622-x
Author Accepted Manuscript (2011)

Generalized Crack Closure Analysis for Elements with Arbitrarily-Placed Side Nodes and Consistent Nodal Forces

John A. Nairn

Received: 30 March 2011 / Accepted: 9 August 2011

Abstract A new approach was developed for the evaluation of energy release rate by the virtual crack closure technique in quadratic and linear elements. The generalized method allows arbitrary placement of the side nodes for quadratic elements and thus includes both standard elements, with mid-side nodes, and singularity elements, with quarter-point nodes, as special cases of one general equation. It also accounts for traction-loaded cracks. The new derivation revealed that the proper nodal forces needed for crack closure calculations should be the newly-defined "nodal edge forces," rather than the global or element forces from standard finite element analysis results. A method is derived for calculating nodal edge forces from global forces. These new forces affect energy release rate calculations for singularity elements and for problems with traction-loaded cracks. Several sample calculations show that the new approach gives improved accuracy.

Keywords Fracture · Finite Elements Analysis · Crack Closure

1 Introduction

The virtual crack closure technique (VCCT) for calculation of energy release rate from finite element analysis (FEA) results including a crack tip was introduced by Rybicki and Kanninen [1977]. Their analysis was for four-node, linear elements. The approach was later extended to higher order elements [Krishnamurthy et al, 1985, Ramamurthy et al, 1986, Raju, 1987, Sethuraman and Maiti, 1988, Narayana et al, 1990], including singularity elements [Barsoum, 1976], and to both 2D and 3D elements (see review by Krueger [2004]). This paper describes a new, generalized crack closure analysis for quadratic and linear elements and for both planar and axisymmetric calculations. The main new feature is that the side-node for quadratic elements can be arbitrarily placed, which allows a single equation to include both mid-side-node and quarter-point elements (*i.e.*, singularity elements) as special cases. Another feature is that crack surfaces are allowed to have traction forces. Although including these tractions is easy, it is rarely done. One often-cited analysis by Raju [1987] includes tractions, but was found to have an error. This new analysis explains why and provides a correction.

The results for mid-side-node elements are identical to prior equations [Krueger, 2004], except for the correction for crack-surface tractions. The approach adopted here, however, demonstrates that the crack-closure calculations can be done without any assumptions about the crack-plane stresses. In other words, prior analyses that used specific fitting functions for stresses [Krishnamurthy et al, 1985, Raju, 1987, Sethuraman and Maiti, 1988] were introducing unnecessary assumptions. When the side node is not in the middle (*e.g.*, quarter-point elements), this new analysis is different then prior literature results. The main difference is that the new approach reveals a modified nodal force that should be used for the crack-closure calculation. The proper forces are neither the element forces nor the global forces that are found in standard FEA output. Rather, the forces must be resolved to "nodal edge force" that are defined by work-equivalence with the crack-plane stress state. A method is described for calculating nodal edge forces from global FEA forces and crack surface trac-

John A. Nairn
Oregon State University, Wood Science & Engineering
112 Richardson Hall, Corvallis, OR 97330, USA
Tel.: +1-541-737-4265
Fax: +1-541-737-3385
E-mail: John.Nairn@oregonstate.edu

tions. The same general approach can be applied to linear elements. The results are trivial and identical to prior equations [Rybicki and Kanninen, 1977], except for the new correction for crack-surface tractions.

Several example calculations are given to test the convergence of mid-side-node elements, quarter-point elements, and linear elements. Converged results were found by extrapolating to zero element size. The mid-side-node elements converged the fastest. The quarter-point elements converged to the same answer when using this new analysis based on nodal edge forces but converged to a different answer when using old methods based on improper forces. The linear elements converged the slowest and 3-node triangular elements converge to different answers.

2 Generalized Crack Closure Analysis

2.1 Crack Closure Integrals

Figure 1 shows the element edges near a crack tip (at node 1 or 3′) in a finite element mesh. For this analysis, the three edges ((1″2″3″), (1′2′3′), and (12±3±)) are assumed to be collinear along the local x axis and the two edges touching the crack tip ((1′2′3′), and (12±3±)) are assumed to have the same length (Δa). The side nodes 2′ and 2± are allowed to be arbitrarily placed along their edges with their positions defined by $R = (x_{2^\pm} - x_1)/\Delta a$ and $R' = (x_{2'} - x_{1'})/\Delta a$. The node placement was limited, however, to symmetric mid-side nodes such that $R' = 1 - R$. The remote edge (1″2″3″) was assumed to have a mid-side node. The analysis presented here could be extended to more general geometries (*e.g.*, non-collinear edges, crack tip edges of different lengths [Krueger, 2004], or non-symmetric nodes), but the results are more complex. Since any crack tip mesh could be created to meet these restrictions, the analysis can be considered sufficiently general. The variable R lets a single analysis apply to conventional quadratic elements with mid-side nodes ($R = 1/2$) and to quarter-point elements ($R = 1/4$).

The standard crack closure integral for total energy release rate in planar analysis with thickness t is:

$$G = \frac{1}{2}\lim_{\Delta a\to 0}\frac{\int_0^{\Delta a}\left[\left(\sigma_{yy}(x') - \sigma_0^{(c)}\right)\Delta v(x)\right]t\,dx}{\int_0^{\Delta a} t\,dx} + \frac{1}{2}\lim_{\Delta a\to 0}\frac{\int_0^{\Delta a}\left[\left(\tau_{xy}(x') - \tau_0^{(c)}\right)\Delta u(x)\right]t\,dx}{\int_0^{\Delta a} t\,dx} \quad (1)$$

where the integration is over the crack surface element, but the stresses are taken from the position $x' = x - \Delta a$ behind the crack tip [Rybicki and Kanninen, 1977]. The first term involving tensile stresses and y-direction

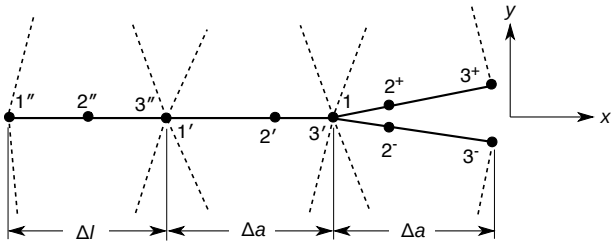

Fig. 1 The nodes and elements around a crack tip at node 1 (or 3′) for a finite element mesh constructed with quadratic elements. The element corner nodes (1 and 1′) will belong to more than one element. The dashed lines indicate one set of boundaries showing three elements above the plane, but those nodes may belong to fewer or more elements without altering the analysis.

crack-opening displacement (COD or $\Delta v(x)$) is mode I or G_I, while the second term with shear stresses and x-direction COD ($\Delta u(x)$) is mode II or G_{II}. The subtraction of $\sigma_0^{(c)}$ and $\tau_0^{(c)}$ allows for constant traction stress on the crack surfaces (note that crack closure can only account for constant crack surface stresses because if those stresses change as the crack propagates, the crack closure integral ceases to be local to the crack tip elements [Nairn, 2000]). Let ξ be a dimensionless variable along the (12±3±) edges such that $\xi = -1$, 0, and +1 at nodes 1, 2± and 3±, respectively. The position and CODs become:

$$x = N_1(\xi)x_1 + N_2(\xi)x_{2^\pm} + N_3(\xi)x_{2^\pm} \quad (2)$$

$$\Delta u(\xi) = N_2(\xi)\Delta u_2 + N_3(\xi)\Delta u_3 \quad (3)$$

$$\Delta v(\xi) = N_2(\xi)\Delta v_2 + N_3(\xi)\Delta v_3 \quad (4)$$

where $N_1(\xi) = -\frac{1}{2}\xi(1-\xi)$, $N_2(\xi) = 1-\xi^2$, and $N_3(\xi) = \frac{1}{2}\xi(1+\xi)$ are quadratic shape functions, and Δu_i and Δv_i are CODs at node $i^\pm$. Transformation of Eq. (1) to the ξ coordinate leads to $G = G_I + G_{II}$ where

$$G_I = \frac{1}{2}\left[\Delta v_2(I_{n0} - I_{n2}) + \frac{\Delta v_3}{2}(I_{n1} + I_{n2})\right] - \frac{\sigma_0^{(c)}}{3}\left[\Delta v_2 + \frac{3-4R}{4}\Delta v_3\right] \quad (5)$$

where

$$I_{nk} = \int_{-1}^{1}\xi^k\sigma_{yy}(\xi')\left(\frac{1}{2} + (1-2R)\xi\right)d\xi \quad (6)$$

and ξ' is dimensionless variable that is $\xi' = -1$, 0, and +1 at nodes 1′, 2′ and 3′, respectively. The result for G_{II} is the same except normal stresses and y CODs are replaced by shear stresses and x CODs. Also the limit as $\Delta a \to 0$ was dropped, but is implicit in all crack closure integrals.

2.2 Nodal Edge Forces

Energy release rate is calculated from FEA results using calculated nodal forces, but the method used to find

those forces is crucial. First, imagine splitting along the crack plane and evaluating the resulting nodal forces associated with the crack plane and crack surface stresses. These forces are denoted as the "nodal edge forces." As explained below they differ from both element forces and global nodal forces, which are the standard forces from FEA output. The only imposed requirement is that the work associated with the edge forces is equal to the work associated with crack-plane stresses, which is the usual condition used when imposing stress-based boundary conditions in FEA. Along the $(1'2'3')$ edge, the edge forces are:

$$\begin{aligned} F_{y,i'} &= t\int_{x_{1'}}^{x_{3'}} N_i(x')\sigma_{yy}(x')dx' \\ &= t\Delta a\int_{-1}^{1} N_i(\xi')\sigma_{yy}(\xi')\left(\frac{1}{2}-(1-2R)\xi'\right)d\xi' \quad (7) \end{aligned}$$

where t is thickness. These forces can be recast as:

$$t\Delta a\begin{pmatrix} I'_{n0}\\ I'_{n1}\\ I'_{n2}\end{pmatrix} = \begin{pmatrix} 1\ 1\ 1\\ -1\ 0\ 1\\ 1\ 0\ 1\end{pmatrix}\begin{pmatrix} F_{y,1'}\\ F_{y,2'}\\ F_{y,3'}\end{pmatrix} = \mathbf{KF} \quad (8)$$

where $\mathbf{K}$ and $\mathbf{F}$ are the matrix and vector and

$$I'_{nk} = \int_{-1}^{1}(\xi')^k\sigma_{yy}(\xi')\left(\frac{1}{2}-(1-2R)\xi'\right)d\xi' \quad (9)$$

Because crack-tip side nodes are symmetrically placed $(R' = 1-R)$, it is easy to derive

$$\xi\big(1+(1-2R)\xi\big)-\xi'\big(1-(1-2R)\xi'\big) = 2(1-2R) \quad (10)$$

$$\left(\frac{1}{2}+(1-2R)\xi\right)d\xi = \left(\frac{1}{2}-(1-2R)\xi'\right)d\xi' \quad (11)$$

which implies $I_{n0} = I'_{n0}$. Multiplying the first relation by $\sigma_{yy}(\xi')$ and integrating gives a relation between I'_{nk} and I_{nk}, which can be rearranged using Eq. (8) to get:

$$\begin{aligned} I_{n1} = \frac{1}{t\Delta a}\Big[&-2RF_{y,1'}+2(1-2R)F_{y,2'} \\ &+2(1-R)F_{y,3'}-(1-2R)t\Delta aI_{n2}\Big] \end{aligned} \quad (12)$$

Substituting this result along with I_{n0} (from I'_{n0} in Eq. (8)) into Eq. (5) provides energy release rate that depends only on nodal edge forces and I_{n2}:

$$\begin{aligned} G_I = \frac{1}{2t\Delta a}\Bigg[&\Delta v_2\Big[F_{y,1'}+F_{y,2'}+F_{y,3'}-t\Delta aI_{n2}\Big] \\ &+\Delta v_3\Big[Rt\Delta aI_{n2}-RF_{y,1'}+(1-2R)F_{y,2'} \\ &+(1-R)F_{y,3'}\Big]\Bigg]-\frac{\sigma_0^{(c)}}{3}\left[\Delta v_2+\frac{3-4R}{4}\Delta v_3\right] \end{aligned} \quad (13)$$

To eliminate I_{n2} as well, a general analysis needs to assume some form for the crack plane stresses (see below on why certain elements do not need any assumptions about stresses). To be consistent with the three independent edge forces, the stress is assumed to have three degrees of freedom or:

$$\sigma_{yy}(\xi') = B_0f_0(\xi')+B_1f_1(\xi')+B_2f_2(\xi') \quad (14)$$

where B_i are three unknown constants (which could be determined from FEA results) and $f_i(\xi')$ are three appropriately chosen functions of ξ' (to be filled in later as needed). The stress integrals become

$$\big(I'_{n0}, I'_{n1}, I'_{n2}\big) = \mathbf{M}\big(B_0, B_1, B_2\big) \quad (15)$$

where the elements of $\mathbf{M}$ are defined by:

$$M_{ij} = \int_{-1}^{1}(\xi')^i f_j(\xi')\left(\frac{1}{2}-(1-2R)\xi'\right)d\xi' \quad (16)$$

The goal is to find I_{n2} which can be recast as:

$$t\Delta aI_{n2} = t\Delta a\big(B_0, B_1, B_2\big)\cdot\mathbf{N} \quad (17)$$

where

$$N_j = \int_{-1}^{1}\xi^2 f_j(\xi')\left(\frac{1}{2}+(1-2R)\xi\right)d\xi \quad (18)$$

Using Eqs. (8) and (15) gives:

$$I_{n2} = \mathbf{NM}^{-1}\mathbf{KF} \quad (19)$$

The energy release rate in terms of nodal edge forces becomes:

$$\begin{aligned} G_I \;=\; &\frac{1}{2t\Delta a}\Big\{\Delta v_2\left[(1,1,1)-\mathbf{NM}^{-1}\mathbf{K}\right]\cdot\mathbf{F} \\ &+\;\Delta v_3\left[(-R,1-2R,1-R)+R\mathbf{NM}^{-1}\mathbf{K}\right]\cdot\mathbf{F}\Big\} \\ &-\frac{\sigma_0^{(c)}}{3}\left[\Delta v_2+\frac{3-4R}{4}\Delta v_3\right] \end{aligned} \quad (20)$$

The result for mode II is identical except that $F_{x,i'}$ replaces $F_{y,i'}$, $\tau_0^{(c)}$ replaces $\sigma_0^{(c)}$, and Δu_i replaces Δv_i.

2.3 Nodal Edge Forces from Global Forces

Forces at the nodes can be defined three different ways as illustrated in Fig. 2. The basic force calculation in FEA is to find an element force, $F_{y,i}^{(ej)}$, which is found from nodal displacements and element stiffness matrix. When a node is shared by several elements, it has several element forces. For example, the crack plane mesh in Fig. 2 shows three elements at each node above the crack plane (with element boundaries indicated by dashed lines, although those nodes may belong to any number of elements without altering this analysis). Thus nodes $1'$ and $3'$ each have multiple element forces, while node $2'$ has only a single element force. The second type of force is a global force, $F_{y,i}^{(g)}$, which is a sum of all element forces on one side of the crack plane; they are

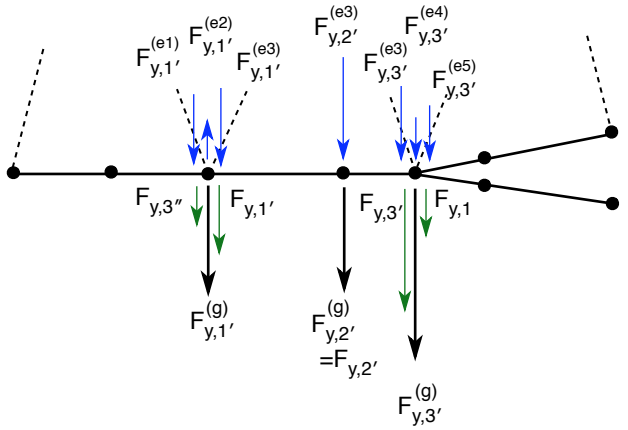

Fig. 2 Forces at the nodes near the crack tip can be resolved into element forces (with superscript (ei)), global forces from the top half plane (with superscript (g)), or nodal edge forces that are consistent with the crack plane stresses (with no superscript).

denoted here as $F^{(g)}_{y,i}$. The analysis in the previous section reveals that neither of these forces are appropriate for crack closure calculation. The proper forces, which are defined as "proper" because they are consistently defined by work-equivalence with the crack plane stress (see Eq. (7)), are the nodal edge forces, $F_{y,i}$. Nodes $1'$ and $3'$ will each have exactly two nodal edges forces and these forces will differ from element forces even when those nodes are only in two elements. The strategy for general crack closure analysis becomes:

1. Using standard FEA methods, calculate all element forces at each node.
2. Sum the forces for all elements on one side of the crack plane to find global nodal forces.
3. Use the methods in this section to partition global forces into nodal edge forces.
4. Substitute edge forces into Eq. (20) to find energy release rate.

The element, global, and edge forces are related by force balance as follows:

$$\begin{pmatrix} \sum_i F^{(ei)}_{y,1'} \\ F^{(e)}_{y,2'} \\ \sum_i F^{(ei)}_{y,3'} \end{pmatrix} = \begin{pmatrix} F^{(g)}_{y,1'} \\ F^{(g)}_{y,2'} \\ F^{(g)}_{y,3'} \end{pmatrix} = \begin{pmatrix} F_{y,1'} + F_{y,3''} \\ F_{y,2'} \\ F_{y,3'} + F_{y,1} \end{pmatrix} \tag{21}$$

Along the $(12^{\pm}3^{\pm})$, the one force that is needed can be evaluated explicitly:

$$\begin{aligned} F_{y,1} &= \sigma_0^{(c)} t\Delta a \int_{-1}^{1} N_1(\xi) \left(\frac{1}{2} + (1-2R)\xi \right) d\xi \\ &= \sigma_0^{(c)} t\Delta a \left(\frac{4R-1}{6} \right) \end{aligned} \tag{22}$$

Along the $(1''2''3'')$, the one force that is needed is

$$F_{y,3''} = \frac{t\Delta l}{2} \int_{-1}^{1} N_3(\xi'') \sigma_{yy}(\xi'') d\xi'' \tag{23}$$

where ξ'' is a dimensionless variable along the $(1''2''3'')$ edge. To keep the VCCT analysis local to the crack-tip elements, $F_{y,3''}$ can be found by extrapolating the crack plane stress from edge $(1'2'3')$:

$$F_{y,3''} = t\Delta a(L_0 B_0 + L_1 B_1 + L_2 B_2) \tag{24}$$

where the L_i are stress integrals over the $(1''2''3'')$ edge:

$$L_i = \frac{\Delta l}{2\Delta a} \int_{-1}^{1} N_3(\xi'') f_i(\xi'') d\xi'' \tag{25}$$

and $f_i(\xi'')$ are the functions in Eq. (14) extended into the second element's coordinate system. Combining Eqs. (8), (15), (22), and (24), the nodal edge forces can be found from standard FEA forces and a known, constant traction stress:

$$\mathbf{F} = \left[\mathbf{I} + \mathbf{L}\mathbf{M}^{-1}\mathbf{K} \right]^{-1} \begin{pmatrix} \\ F^{(g)}_{y,1'} \\ F^{(g)}_{y,2'} \\ F^{(g)}_{y,3'} - \frac{(4R-1)t\Delta a\sigma_0^{(c)}}{6} \end{pmatrix} \tag{26}$$

where $\mathbf{I}$ is the identity matrix and the $\mathbf{L}$ matrix has (L_0, L_1, L_2) on the first row and zeros elsewhere. The matrix $\left[\mathbf{I} + \mathbf{L}\mathbf{M}^{-1}\mathbf{K} \right]^{-1}$ simplifies to the identity matrix with first row replaced by (D_0, D_1, D_2), which depend on L_i and are readily evaluated for any element type. The nodal edge forces thus reduce to:

$$\mathbf{F} = \begin{bmatrix} D_0 F^{(g)}_{y,1'} + D_1 F^{(g)}_{y,2'} + D_2 \left(F^{(g)}_{y,3'} - \frac{(4R-1)t\Delta a\sigma_0^{(c)}}{6} \right) \\ F^{(g)}_{y,2'} \\ F^{(g)}_{y,3'} - \frac{(4R-1)t\Delta a\sigma_0^{(c)}}{6} \end{bmatrix} \tag{27}$$

The forces for mode II replace y forces with x forces and replace $\sigma_0^{(c)}$ with $\tau_0^{(c)}$. Substituting this $\mathbf{F}$ into Eq. (20) provides the final, general crack closure result in terms of global nodal forces and nodal CODs.

This important result gives a procedure for finding nodal edge forces from typical FEA output for global forces and a known traction stress. The largest effect is in finding $F_{y,1'}$. Thus any prior crack closure method that depends on $F_{y,1'}$ should be revised to use the edge forces calculated here. A second effect arises for traction loaded cracks. The general equation (see Eq. (20)) has a traction term that was derived by integrating forces along $(12^{\pm}3^{\pm})$ edge. This term is identical to the traction effect added by Raju [1987]. When the forces along the $(1'2'3')$ are treated consistently with the traction forces, however, a second traction term appears (see first and third row in Eq. (27)). When both effects are combined, the final effect of tractions is different then prior results [Raju, 1987].

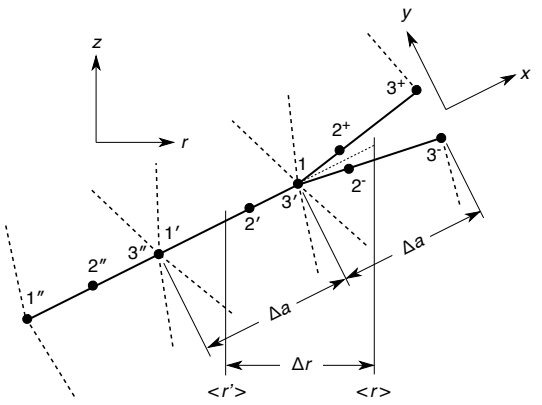

Fig. 3 Crack plane nodes and edges for a crack in an axisymmetric analysis. The x used in the analysis remains along the crack path, the crack may be tilted with respect to the global r and z axes. $\Delta r = \langle r \rangle - \langle r' \rangle$ is the difference between the radial-coordinate midpoints of the two edges at the crack tip.

2.4 Axisymmetric Analyses

The crack plane edges for an axisymmetric analysis are shown in Fig. 3. As in the planar analysis, the x axis is defined as along the crack path. The crack orientation, however, may be tilted from the global r and z axes, and, unlike planar analyses, the axisymmetric results depend on this crack orientation. The crack orientation is defined by the radial coordinates at the midpoint of the $(1'2'3')$ and the $(12^{\pm}3^{\pm}))$, which are denoted by $\langle r' \rangle$ and $\langle r \rangle$, respectively. The radial distance between these points is $\Delta r = \langle r \rangle - \langle r' \rangle$. For axial cracks (*i.e.*, cracks propagating in the z direction) Δr will be zero, but for all other cracks, it will be nonzero with a maximum of $\Delta r = \Delta a$ for radial cracks.

The crack closure analysis for axisymmetric problems is nearly identical to the planar analysis. The procedure is to replace incremental area $t\,dx$ in Eq. (1) by the polar integration area or $2\pi r(x')\,dx$. Note that $r(x')$ is most appropriately referenced to the $(1'2'3')$ edge because this area times the stress is providing the force to the energy calculation. The subsequent analysis up to the general result in Eq. (20) is nearly identical, with three exceptions. First, t is replaced by $\langle r' \rangle$. Second, the **F**, **M**, and **N** definitions include radial position in the integrand:

$$F_{y,i'} = \Delta a \int_{-1}^{1} r(\xi') N_i(\xi') \sigma_{yy}(\xi') \left(\frac{1}{2} - (1-2R)\xi' \right) d\xi' \tag{28}$$

$$M_{ij} = \frac{1}{\langle r' \rangle} \int_{-1}^{1} (\xi')^i r(\xi') f_j(\xi') \left(\frac{1}{2} - (1-2R)\xi' \right) d\xi' \tag{29}$$

$$N_j = \frac{1}{\langle r' \rangle} \int_{-1}^{1} \xi^2 r(\xi') f_j(\xi') \left(\frac{1}{2} + (1-2R)\xi \right) d\xi \tag{30}$$

(Note: the forces in axisymmetric analyses are taken as force per radian.) Third, the explicit integration for crack tractions (last term in Eq. (5)) changes to:

$$-\frac{\sigma_0^{(c)}}{3} \left[\left(1 - \frac{(1-2R)}{5} \frac{\Delta r}{\langle r' \rangle} \right) \Delta v_2 + \left(\frac{3-4R}{4} + \frac{(5+8R(1-2R))}{40} \frac{\Delta r}{\langle r' \rangle} \right) \Delta v_3 \right] \tag{31}$$

This new constant stress term reduces to the planar analysis result for axial cracks ($\Delta r = 0$), but for other crack orientations the constant stress effect depends on orientation.

The analysis for finding nodal edge forces from global forces is also nearly identical, with two exceptions. First the extrapolation terms add radial position to the integrand:

$$L_i = \frac{\Delta l}{2 \langle r' \rangle \Delta a} \int_{-1}^{1} N_3(\xi'') r(\xi'') f_i(\xi'') d\xi'' \tag{32}$$

Second, the explicit integral to account for constant crack surface tractions changes the $F_{y,1}$ term subtracted from $F^{(g)}_{y,3'}$ in Eq. (27):

$$F_{y,1} = \sigma_0^{(c)} \Delta a \langle r' \rangle \left[\frac{4R-1}{6} + \frac{16R(1+R)-7}{60} \frac{\Delta r}{\langle r' \rangle} \right] \tag{33}$$

3 Specific Elements

3.1 Mid-Side Nodes

Applying the general result to mid-side elements with $R = 1/2$, results in **N** being equal to the last row of **M** ($N_j = M_{2j}$). Thus, $\mathbf{N}\mathbf{M}^{-1} = (0, 0, 1)$ (*i.e.*, last row of the identity matrix) and $\mathbf{N}\mathbf{M}^{-1}\mathbf{K} = (1, 0, 1)$. The energy release rate simplifies to

$$G_I = \frac{1}{2t\Delta a} \left[\Delta v_2 F^{(g)}_{y,2'} + \Delta v_3 F^{(g)}_{y,3'} \right] - \frac{\sigma_0^{(c)}}{3} \left[\Delta v_2 + \frac{\Delta v_3}{2} \right] \tag{34}$$

The first term is the usual result quoted for mid-side elements [Krueger, 2004]; the second terms corrects G_I for constant, crack-surface traction. Raju [1987] also included tractions but had the last term as $\Delta v_3/4$ instead of $\Delta v_3/2$. As explained above, the error in Raju [1987] was caused by inconsistent treatment of forces. This new result is verified below as being more accurate in calculations for a pressure loaded crack.

The axisymmetric analysis is similar, except the constant traction term changes for non-axial cracks:

$$G_I = \frac{1}{2\left\langle r' \right\rangle \Delta a}\left[\Delta v_2 F^{(g)}_{y,2'} + \Delta v_3 F^{(g)}_{y,3'}\right] - \frac{\sigma_0^{(c)}}{3}\left[\Delta v_2 + \frac{\Delta v_3}{2}\left(1 + \frac{\Delta r}{2\left\langle r' \right\rangle}\right)\right] \quad (35)$$

Notably, these mid-side node results do not depend on D_i, which implies that the final energy release rate is independent of the assumptions used for stress in the crack plane. Prior analyses of this element included assumptions about the variation in crack plane stress [Krishnamurthy et al, 1985, Raju, 1987, Sethuraman and Maiti, 1988]. This analysis shows those assumptions are irrelevant and explains why those using different assumptions got the same result. The only assumption actually needed is a work equivalence between nodal edge forces and integrated stress (*i.e.*, Eq. (7)).

3.2 Quarter-Point Elements

In planar, quarter-point elements ($R = 1/4$), the distance from the crack tip along the $(1'2'3')$ edge, r, is

$$r = \frac{\Delta a}{4}(1 - \xi')^2 \quad (36)$$

The intention of quarter-point elements is to represent a singular stress state. Thus a logical assumption for the crack-plane stress is to use the first three terms of a Williams [1957] series expansion of crack-tip stresses:

$$\sigma_{yy}(r_c) = \frac{B_0\sqrt{\Delta a}}{2\sqrt{r}} + B_1 + \frac{2B_2\sqrt{r}}{\sqrt{\Delta a}} \quad (37)$$

where B_i are determined from FEA results. In the dimensionless coordinates the expansion is:

$$\sigma_{yy}(\xi') = \frac{B_0}{1 - \xi'} + B_1 + B_2(1 - \xi') \quad (38)$$

The expansion functions in the generalized crack closure analysis become:

$$f_0(\xi') = \frac{1}{1 - \xi'},\ f_1(\xi') = 1,\ \text{and}\ f_2(\xi') = 1 - \xi' \quad (39)$$

Substituting $f_i(\xi')$ into M_{ij} and N_j leads to difficult integrals, but they can be evaluated explicitly (using *Mathematica* [Wolfram Research, 2009]):

$$M_{ij} = \frac{\Gamma(1+i)\Gamma(1+j)}{2\Gamma(2+i+j)} + \frac{(-1)^i {}_2\mathrm{F}_1(1+i, -j, 2+i, -1)}{2\,(1+i)} \quad (40)$$

$$N_j = \frac{4^{\frac{j}{2}}}{1+j} + \frac{8\left(4^{\frac{j}{2}}\right)}{3+4j+j^2} - \frac{4^{\frac{j}{2}}\sqrt{\pi}\,\Gamma(\frac{1+j}{2})}{\Gamma(2+\frac{j}{2})} \quad (41)$$

where $\Gamma(x)$ is the Gamma function and ${}_2\mathrm{F}_1(a, b, c, x)$ is the Hypergeometric Function (see Arfken [1970], pg. 638). The exact evaluations are:

$$\mathbf{M} = \begin{bmatrix} 1 & 1 & \frac{4}{3} \\ 0 & -\frac{1}{3} & -\frac{2}{3} \\ \frac{1}{3} & \frac{1}{3} & \frac{8}{15} \end{bmatrix} \text{ and } \mathbf{N} = \left(\frac{11}{3} - \pi, \frac{1}{3}, \frac{52}{15} - \pi\right) \quad (42)$$

The crack closure results in terms of nodal edge forces become

$$G_I = \frac{1}{2t\Delta a}\left\{\Delta v_2\left(\frac{21\pi}{2} - 32, 17 - \frac{21\pi}{4}, \frac{33\pi}{2} - 52\right)\cdot\mathbf{F} + \Delta v_3\left(8 - \frac{21\pi}{8}, \frac{21\pi}{16} - \frac{7}{2}, 14 - \frac{33\pi}{8}\right)\cdot\mathbf{F}\right\} - \frac{\sigma_0^{(c)}}{3}\left(\Delta v_2 + \frac{\Delta v_3}{2}\right) \quad (43)$$

These coefficient vectors are identical to the coefficients found in some previous analyses of quarter-point elements [Ramamurthy et al, 1986, Raju, 1987, Narayana et al, 1990], but those analyses did not notice the need for nodal edge forces. Ramamurthy et al [1986] gives no specifics on forces, which implies they used global forces. Raju [1987] explicitly says to sum forces for all elements to get global forces. Narayana et al [1990] claims global forces should be used for $F_{y,2'}$ and $F_{y,3'}$, but specified use of element force for $F_{y,1'}$. The new result here is to use nodal edge forces.

Both Sethuraman and Maiti [1988] and Raju [1987] obtain results (albeit different results) that do not depend on $F_{y,1'}$ by assuming a stress state that depends only on two unknowns rather than three:

$$\sigma_{yy}(\xi') = \frac{B_0}{1 - \xi'} + B_1 \quad (44)$$

Because this stress function has only two parameters, the final answer can be expressed in terms of only two forces — $F_{y,2'}$ and $F_{y,3'}$. In essence, this simplification is solving for $F_{y,1'}$ in terms of $F_{y,2'}$ and $F_{y,3'}$, which might eliminate the need to resolve nodal edge forces at node $1'$. Because the fitting function for stress has fewer unknowns (two instead of three), however, this approximation with extra constraints should always be less accurate that a three-parameter model based on three correctly-calculated nodal edges forces. In a seeming contradiction, Sethuraman and Maiti [1988] claimed the simplified equation is more accurate than the full-force method in Ramamurthy et al [1986], Narayana et al [1990] and Raju [1987]. This contradiction is resolved by noting that they used the wrong force at node $1'$. In other words, a simplified equation that calculates $F_{y,1'}$ from $F_{y,2'}$ and $F_{y,3'}$ could be more accurate then a three-force analysis that uses the wrong force for $F_{y,1'}$, but a three-force analysis that uses consistent forces should be best of all.

This new analysis is not complete until edge forces are found and those forces depend on L_j. Along the $(1''2''3'')$ edge (which has a mid-side node or $R'' = 1/2$), the distance from the crack tip is

$$r = \Delta a \left(1 + (1-\xi'')\frac{\Delta l}{2\Delta a}\right) \tag{45}$$

Extrapolating the crack-plane stresses from the $(1'2'3')$ edge, the required fitting functions along the $(1''2''3'')$ edge are:

$$f_0(\xi'') = \frac{1}{2\sqrt{1+\frac{(1-\xi'')\Delta l}{2\Delta a}}}, \quad f_1(\xi'') = 1, \text{ and}$$
$$f_2(\xi'') = 2\sqrt{1+\frac{(1-\xi'')\Delta l}{2\Delta a}} \tag{46}$$

The L_j integrals can be evaluated analytically (using *Mathematica* [Wolfram Research, 2009]):

$$L_0 = -\frac{16+30\chi+15\chi^2}{15\chi^2} + \frac{16+22\chi+6\chi^2}{15\chi^2}\sqrt{1+\chi} \tag{47}$$
$$L_1 = \frac{1}{6}\chi \tag{48}$$
$$L_2 = -\frac{64+168\chi+140\chi^2}{105\chi^2} + \frac{64+136\chi+80\chi^2+8\chi^3}{105\chi^2}\sqrt{1+\chi} \tag{49}$$

where $\chi = \Delta l/\Delta a$. Furthermore, explicit evaluation of $\left[\mathbf{I}+\mathbf{L}\mathbf{M}^{-1}\mathbf{K}\right]^{-1}$ leads to

$$D_0 = \frac{1}{D}, \quad D_1 = \frac{1}{2} - \frac{2+\chi}{4D}, \quad \text{and}$$
$$D_2 = -1 + \frac{1-6L_0+\chi}{D} \tag{50}$$

where $D = 1 + 3L_0 - 12L_1 + (15L_2/2)$ or

$$D = -\frac{272+630\chi+420\chi^2+70\chi^3}{35\chi^2} + \frac{272+494\chi+242\chi^2+20\chi^3}{35\chi^2}\sqrt{1+\chi} \tag{51}$$

Substituting these results into Eq. (27) gives the nodal forces, which when substituted into Eq, (20) gives the energy release rate. This result is new and tedious, but numerically trivial and essential when doing crack closure calculations with quarter-point elements.

For axisymmetric calculations, the radial position along the $(1'2'3')$ edge is

$$\frac{r(\xi')}{\langle r'\rangle} = 1 + \frac{\Delta r}{2\langle r'\rangle}\left(1 - \frac{1}{2}(1-\xi')^2\right) \tag{52}$$

Using the same $f_i(\xi')$ as for planar elements, the axisymmetric versions of M_{ij} and N_j can be explicitly evaluated

$$\mathbf{M} = \begin{bmatrix} 1+\frac{\Delta r}{6\langle r'\rangle} & 1 & \frac{4}{3}-\frac{2\Delta r}{15\langle r'\rangle} \\ \frac{\Delta r}{6\langle r'\rangle} & -\frac{1}{3}+\frac{2\Delta r}{15\langle r'\rangle} & -\frac{2}{3}+\frac{\Delta r}{5\langle r'\rangle} \\ \frac{1}{3}+\frac{\Delta r}{30\langle r'\rangle} & \frac{1}{3}-\frac{\Delta r}{15\langle r'\rangle} & \frac{8}{15}-\frac{16\Delta r}{105\langle r'\rangle} \end{bmatrix} \tag{53}$$

$$\mathbf{N} = \left(\frac{11}{3} - \pi + \frac{\Delta r}{\langle r'\rangle}\left(\frac{29}{30}-\frac{\pi}{4}\right), \frac{1}{3}+\frac{\Delta r}{15\langle r'\rangle}, \frac{52}{15}-\pi+\frac{2\Delta r}{105\langle r'\rangle}\right) \tag{54}$$

For crack planes in the z direction in the r-z axisymmetric coordinate system, $\Delta r = 0$ and the axisymmetric results reduce to the planar results (except t is replaced by $\langle r'\rangle$). For cracks in any other direction $\Delta r \neq 0$ and the equations get exceedingly complex. The complete results can be found by application of the generalized results, but are not given here and are not available in the literature. A potential simplification to avoid further analysis is to ignore the Δr terms. In calculations with a highly refined mesh, the results for a full $\Delta r \neq 0$ analysis should converge to the same results as a $\Delta r = 0$ analysis because $\Delta r \to 0$ as $\Delta a \to 0$. This approach should be used with caution because the rate of convergence might be affected. A better option for $\Delta r \neq 0$ cracks might be to avoid quarter-point elements and use mid-side-node elements instead.

3.3 Linear Elements

A similar generalized analysis can be done for linear elements (*e.g.*, elements with nodes on the corners but no side nodes). Because most of the complication in quadratic edges was due to placement of the side nodes, the linear analysis is much simpler. Furthermore, like the mid-side-node elements, a final result can be found without any assumptions about crack-plane stresses. The results are identical to prior literature result [Rybicki and Kanninen, 1977, Krueger, 2004], except for a change in the crack-surface traction term. The result for planar, linear elements is:

$$G_I = \frac{F^{(g)}_{y,3'}\Delta v_3}{2t\Delta a} - \frac{\sigma_0^{(c)}\Delta v_3}{2} \tag{55}$$

The result for axisymmetric, linear elements is

$$G_I = \frac{F^{(g)}_{y,3'}\Delta v_3}{2\langle r'\rangle\Delta a} - \frac{\sigma_0^{(c)}\Delta v_3}{2}\left(1+\frac{\Delta r}{2\langle r'\rangle}\right) \tag{56}$$

As for the mid-side-node elements, the traction terms here differ from Raju [1987], where the traction term was $\sigma_0^{(c)}\Delta v_3/4$ rather than $\sigma_0^{(c)}\Delta v_3/2$. The error in Raju [1987] was inconsistent treatment of the force at the crack tip node.

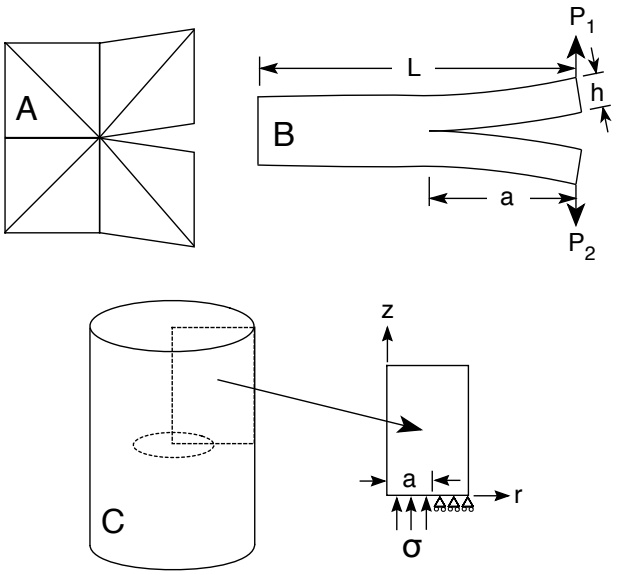

Fig. 4 A. The arrangement of triangular elements at the crack tip. B. Geometry for double cantilever beam calculations. C. Axisymmetric analysis of a pressure-loaded, penny-shaped crack in a cylinder.

4 Results and Discussion

The crack closure equations were verified by several examples. The FEA calculations were done with 3 node linear triangles, 4 node linear quadrilaterals, 6 node quadratic triangles, 8 node quadratic quadrilaterals, and 9 node quadrilateral Lagrangian elements. The latter 3 were done with either mid-side nodes or quarter-point nodes. To compare to prior quarter-point methods, calculations with those elements were repeated by using global or element forces [Krishnamurthy et al, 1985, Ramamurthy et al, 1986, Raju, 1987] or by using simplified equations that avoid $F_{y,1'}$ [Raju, 1987, Sethuraman and Maiti, 1988]. For 3 and 6-node triangular elements, the squares were divided into two triangles. At the crack tip, the triangular elements were arranged as shown in Fig. 4A. For quarter-point elements, the side node along each edge emanating from the crack tip was moved to the quarter-point position. All calculations were done with open-source FEA software [Nairn, 2011] and post-processed with custom software to implement the different equations.

Although common FEA practice would use smaller elements near the crack tip, here all analyses were done with a regular mesh of constant-sized, square elements. The triangular elements divided the squares into two right, isosceles triangles. This approach tended to give more consistent convergence results, especially when comparing different element types. For each example and each element type a series of about 10 calculations with decreasing element size were run. A converged result for infinite elements was estimated by extrapolating those results to zero element size. Common practice in crack closure studies is to compare results to analytical solutions. For finite-sized specimens, however, such analytical solutions are themselves approximate and therefore may not provide the best test. Here, the results were compared to analytical results, but the main criterion for verification was that all elements converged to the same answer.

4.1 DCB Mode I, Mode II, and Mixed Mode

Figure 4B shows a double cantilever beam specimen. Mode I conditions used $P_1 = -P_2$, mode II used $P_1 = P_2$, and mixed mode used $P_2 = 0$. The results for mixed mode were a superposition of mode I and II results, and therefore only pure mode I and II results are discussed. The specimen had length $L = 40$ mm with arms of $h = 2$ mm. The crack tip was in the middle ($a = 20$ mm). The meshes varied from 2 elements through the thickness of the arms up to 20 elements for mode I and 24 elements for mode II. The smallest square-element sizes were 0.1 mm for mode I and 0.083 mm for mode II.

The mode I results are given in Figs. 5 and 6 and were normalized to the simple beam theory result:

$$G_{beam} = \frac{12P^2a^2}{B^2Eh^3} \tag{57}$$

where P is load, B is thickness, and E is modulus of the isotropic material. The quadratic elements (6, 8, and 9 node) with mid-side nodes worked best. They converged rapidly and all converged to the same answer. This result was judged to be the correct result. Further verification is found by comparing to a corrected beam theory that accounts for shear deformation and crack root rotation during delamination with isotropic arms [Williams, 1989]:

$$\frac{G_I}{G_{beam}} = \left(1 + 0.67\frac{h}{a}\right)^2 = 1.1385 \tag{58}$$

This analytical result is within 0.06% of the FEA result for 8 and 9 node elements, both of which gave 1.1392 when extrapolated to zero element size.

The results for other elements were judged by how they compared to the above result. The 4 node linear element converged to the same answer, but required smaller elements to get good results. The 3 node linear element converged to a different answer. To check if the 3 node convergence might turn toward the correct answer, the mesh size was reduced further down to 0.04 mm elements, but the results showed no indication of changing direction.

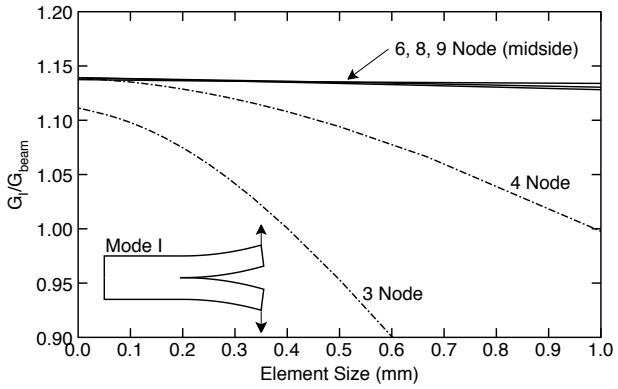

Fig. 5 Mode I energy release rates normalized to simple beam theory as a function of element size. The solid lines are for quadratic elements with mid-side nodes. The dash-dot lines are for linear elements.

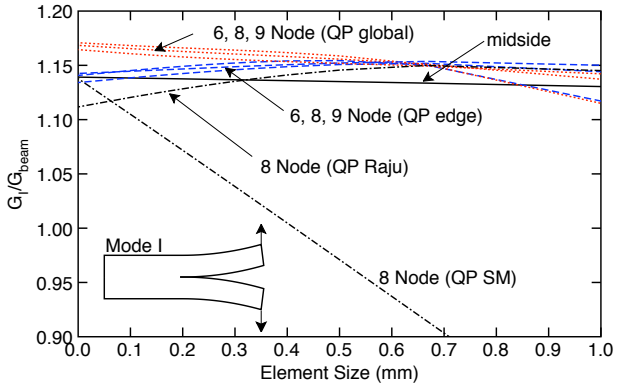

Fig. 6 Mode I energy release rates normalized to simple beam theory as a function of element size. The dashed lines are for quarter-point elements based on nodal edge forces ("QP edge"). The dotted lines are for quarter-point elements using global nodal forces ("QP global"). The dash-dot lines are for two simplified quarter-point element equations ("QP Raju" and "QP SM"). The solid line is reference result for quadratic elements with mid-side nodes.

Figure 6 shows results for quarter-point elememts. When those elements used nodal edge forces as advocated here ("QP edge"), they all converged to the correct result. When those elements used global forces instead of edge forces, however, they converged to a different result ("QP global"). Calculations were also done using element force at node 1′; they differed the most from other results (not shown in the figure). The simplified quarter-point results by Raju [1987] or by Sethuraman and Maiti [1988] are labeled "QP Raju" and "QP SM" respectively. The Raju [1987] method converged to a different answer. The Sethuraman and Maiti [1988] method converged to the same result as other elements, but converged very slowly.

In summary, all elements using the current equations, except the 3 node linear elements, converged to the same answer within 0.44%. Calculations for quarter-point elements based on global force or using one simplified analysis [Raju, 1987] differed by 2.2% to 2.8%. A second simplified, quarter-point analysis [Sethuraman and Maiti, 1988] was accurate but only in the extrapolated limit for zero element size. It was the *least* accurate method for any mesh with non-zero element size, where it differed by more than 3.0% for elements 0.1 mm or larger.

The mode II results are given in Fig. 7 and were normalized to the simple beam theory result:

$$G_{beam} = \frac{9P^2a^2}{B^2Eh^3} \tag{59}$$

The convergence performance is similar to mode I, but not as clear cut. Again, the quadratic elements (6, 8, and 9 node) with mid-side nodes converged rapidly and all converged to the same answer. A corrected, mode II beam theory [Wang and Williams, 1992] predicts:

$$\frac{G_I}{G_{beam}} = \left(1 + \sqrt{\frac{11}{63}} * 0.67\frac{h}{a}\right)^2 = 1.0568 \tag{60}$$

The converged FEA result for 8 and 9 node elements was 1.0423, which differs from analytical solution by 1.4%. The well-converged, FEA result was judged to be the correct result (*i.e.*, more accurate than corrected beam theory) and therefore was used to verify other elements. The 4 node linear element converged slowly to the same answer. The 3 node triangles got closer than for mode I, but was still slightly different. The results for quarter-point elements were more varied. When done using the nodal edge forces as advocated here ("QP edge"), they varied from other elements, but were near the expected answer. When using global forces ("QP global"), they were systematically higher than other elements. The simplified quarter-point element methods were not tested in mode II.

4.2 Penny Shaped Crack

Figure 4C shows a centered, penny-shaped crack having internal pressure, σ, on the crack surfaces. This problem is an axisymmetric analysis with crack orientation off the z axis (*i.e.*, $\Delta r \neq 0$) and has crack surface tractions (the pressure); it was chosen to test those terms in the analysis. Because the equations for quarter-point elements when $\Delta r \neq 0$ were not derived, these calculations included only mid-side-node elements and linear elements. The number of elements across the cylinder was varied from 4 to 40, which resulted it smallest element size of 0.05 mm.

Figures 8 and 9 give the results for two different boundary conditions on the vertical surface of the cylinder — zero displacement or zero stress. The cylinder

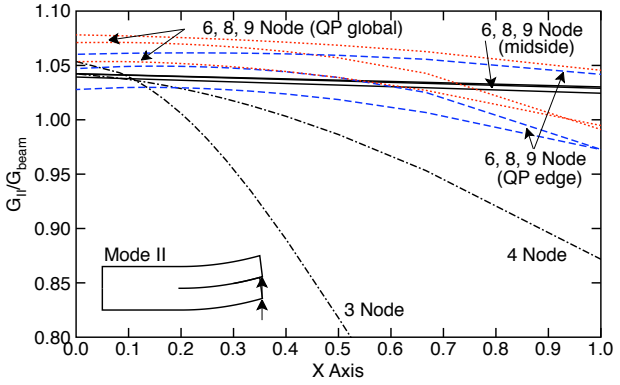

Fig. 7 Mode II energy release rates normalized to simple beam theory as a function of element size. The solid lines are for quadratic elements with mid-side nodes. The dashed lines are for quarter-point elements based on nodal edge forces defined here ("QP edge"). The dotted lines are for quarter-point elements using global nodal forces ("QP global"). The dash-dot lines are for linear elements.

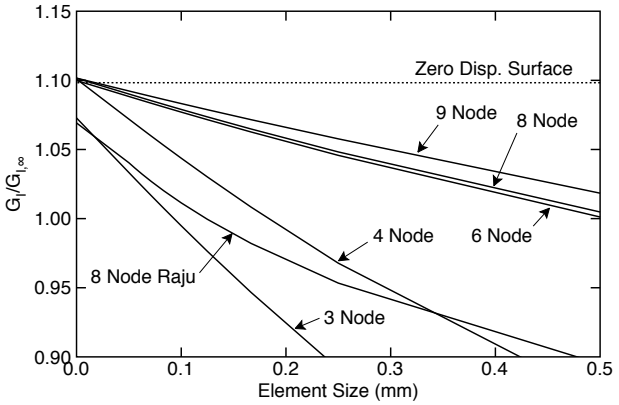

Fig. 8 Mode I energy release rate for extension of a penny shaped crack with zero displacement on the cylinder's outer, vertical surface. The isotropic material properties were $E = 2.3$ GPa and $\nu = 0.25$. The horizontal dashed line is a semi-analytical solution.

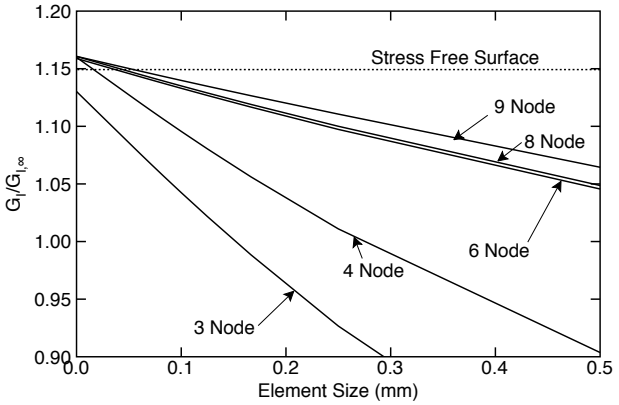

Fig. 9 Mode I energy release rate for extension of a penny shaped crack with zero stress on the cylinder's outer, vertical surface. The isotropic material properties were $E = 2.3$ GPa and $\nu = 0.25$. The horizontal dashed line is a semi-analytical solution.

was 10 mm long with a 2 mm radius. The crack radius was $a = 1$ mm. All results were normalized to energy release rate for a pressure loaded crack in an infinite sheet [Sneddon and Lowengrub, 1969]:

$$G_{I,\infty} = \frac{4(1-\nu^2)a\sigma^2}{\pi E} \tag{61}$$

where ν is Poisson's ratio. The 4, 6, 8, and 9 node elements all converged to the same answer. The quadratic elements (6, 8, and 9 nodes) converged faster than the linear element (4 node). The 3 node triangles converged to a different answer. Note that most elements converged slower for the penny-shaped cracks then for the bending problems. The slower convergence is likely due to the displacement field. In particular, quadratic elements can accurately describe bending displacements with relatively large elements, but need smaller elements for similar accuracy in the pressure-loaded crack displacements.

Sneddon and Tait [1963] and Sneddon and Lowengrub [1969] derived finite-radius correction factors in a semi-analytical model:

$$\frac{G_I}{G_{I,\infty}} = \left(1 + \frac{\eta_1}{100}\right)^2 \text{ and } \frac{G_I}{G_{I,\infty}} = \left(1 + \frac{\eta_2}{100}\right)^2 \tag{62}$$

where η_1 and η_2 are for zero displacement or zero stress on the vertical surface of the cylinder. The dotted lines in Figure 8 show the numerically evaluated results for $a/R = 0.5$ of $\eta_1 = 4.8$ and $\eta_2 = 7.2$. These values agree well with extrapolated limit for 4, 6, 8, and 9 node elements.

To verify the new crack-surface traction result *vs.* the previous analysis by Raju [1987], calculations were run with both equations. The line labeled "8 Node Raju" for zero-displacement boundary conditions (in Fig. 8) shows that the prior traction method converges to a different answer and differs from the analytical solution. The zero-size intercept was found by extrapolating a cubic fit to finite-element-size results. The "8 Node" line uses the same element but the new traction terms. It converges faster and agrees better with the analytical solution.

5 Conclusions

A subtle, but important, aspect of crack closure calculations is to treat nodal forces consistently with the rest of the analysis. The actual or implied assumption of all crack closure methods is that nodal forces along the $(1'2'3')$ edge ahead of the crack tip (see Fig. 1) are related to crack plane stresses by the work-equivalence in Eq. (7). As a consequence, the proper forces for calculations are the forces termed here as the "nodal

edge forces" and not the global or element forces used in prior crack closure analyses. In other words, prior crack closure calculations are technically wrong, but can be fixed by calculating nodal edge forces. The switch to nodal edge forces, does not affect all methods. Fortunately, prior equations for linear elements or quadratic elements [Krueger, 2004] are correct, provided they did not attempt to account for crack surface tractions. They are correct because the global forces and nodal edge forces needed for those calculations are the same. In contrast, any prior analysis that either depends on the force one element away from the crack tip (*i.e.*, on $F_{y,1'}$) or has crack surface tractions should be corrected. The corrections are only a few percent (which may explain why the errors were not noticed before), but are recommended for increased accuracy and improved convergence.

A dependence on $F_{y,1'}$ only appears when the node is moved from the midpoint, such as for quarter-point elements. The results here show that some prior methods for quarter-point elements have the right equation [Krishnamurthy et al, 1985, Ramamurthy et al, 1986, Raju, 1987], but they give inaccurate results when implemented using global forces. By correcting that analysis to use nodal edge forces as defined in Eq. (27), the quarter-point elements give improved results. Two prior methods derived simplified quarter-point element results that eliminated $F_{y,1'}$. The extra approximations needed for these methods makes them less accurate than the full equation with proper nodal edge forces. Despite the fact that quarter-point elements were developed to more accurately represent crack tip stresses [Barsoum, 1976], their overall convergence performance is inferior to the corresponding element with mid-side nodes. The reasons for inferior convergence with quarter point elements are uncertain. It could be that the shape functions that are providing a singular strain state for those elements might be causing numerical issues when needed for calculations involving spatial coordinates (because isoparametric elements use the same shape functions for both displacements and spatial coordinates).

The distinction between nodal edge forces and global forces also changes the net effect of crack surface tractions. One prior analysis added crack-surface traction effects by accounting for their work on the crack surface [Raju, 1987]. But when resolving global forces into nodal edge forces, those tractions have an additional effect on the crack tip force (see $F_{y,3'}$ in Eq. (27)). When both these effects are included, the net effect of crack-surface tractions changes. The example calculation for a penny-shaped crack loaded by pressure shows the new result is more accurate.

References

Arfken G (1970) Mathematical Methods for Physists. Academic Press, New York

Barsoum RS (1976) On the use of isoparametric finite elements in linear fracture mechanics. Int J Num Meth Engng 10:25–37

Krishnamurthy T, Ramamurthy TS, Vijayakumar K, Dattaguru B (1985) Modified crack closure integral method for higher order finite elements. In: Proc. Int. Conf. Finite Elements in Computational Mechanics, pp 891–900

Krueger R (2004) Virtual crack closure technique: History, approach, and applications. Applied Mechanics Reviews 57(2):109–142

Nairn JA (2000) Exact and variational theorems for fracture mechanics of composites with residual stresses, traction-loaded cracks, and imperfect interfaces. Int J Fract 105:243–271

Nairn JA (2011) Material point method (NairnMPM) and finite element analysis (NairnFEA) open-source software. URL http://code.google.com/p/nairn-mpm-fea/

Narayana KB, Dattaguru B, Ramamurthy TS, Vijayakumar K (1990) Modified crack closure integral using six-noded isoparametric quadrilaterial singular elements. Eng Fract Mech 36:945–955

Raju IS (1987) Calculation of strain-energy release rates with higher order and sigular finite elements. Eng Fract Mech 28(3):251–274

Ramamurthy TS, Krishnamurthy T, Narayana KB, Vijayakumar K, Dattaguru B (1986) Modified crack closure integral method with quarter point elements. Mechanics Research Communications 13:179–186

Rybicki EF, Kanninen MF (1977) A finite element calculation of stress intensity factors by a modified crack closure integral. Eng Fract Mech 9:931–938

Sethuraman R, Maiti SK (1988) Finite element based computation of strain energy release rate by modified crack closure integral. Eng Fract Mech 30:227–331

Sneddon IN, Lowengrub M (1969) Crack Problems in the Classical Theory of Elasticity. John Wiley & Sons, New York

Sneddon IN, Tait RJ (1963) The effect of a penny-shaped crack on the distibution of stress in a long cylinder. Int J Engng Sci 1:391–409

Wang Y, Williams JG (1992) Corrections for mode ii fracture toughness specimens of isotropic materials. Comp Sci & Tech 43:251–256

Williams JG (1989) End corrections for orthotropic dcb specimens. Comp Sci & Tech 35:367–376

Williams ML (1957) On the stress distribution at the base of a stationary crack. J Appl Mech 24:109–114

Wolfram Research (2009) Mathematica 7.0. Champaign, IL